IEEE Access
Multidisciplinary | Rapid Review | Open Access Journal

Date of publication xxxx 00, 0000, date of current version xxxx 00, 0000.

Digital Object Identifier 10.1109/ACCESS.2022.Doi Number

Robust Scheduling of a Hybrid Hydro/ photovoltaic/Pumped-Storage System for Multiple Grids Peak-Shaving and Congestion Management

HONG ZHOU [1], LIANG LU[1], MINGKUI WEI, LI SHEN, and YOUBO LIU, Member, IEEE

[1]Southwest Branch, State Grid Corporation of China, Chengdu, CO 610095 China
[2]College of Electrical Engineering, Sichuan University, Chengdu, CO 610065 China

Corresponding author: YOUBO LIU (e-mail: liuyoubo@scu.edu.cn).

This work was supported by the Southwest Branch of State Grid Corporation of China under Grant SGSW0000FZGHBJS2200070

ABSTRACT Southwest China possesses substantial hydropower potential and abundant solar resources. To harness these renewable resources effectively, extensive photovoltaic (PV) facilities and cascaded hydropower stations have been strategically constructed in mountainous regions, culminating in the development of hybrid energy systems (HES) that combine hydro, PV, and pumped-storage. Nevertheless, the current research on HES scheduling often neglects the transmission congestion in the local grid to which HES is connected. This oversight results in avoidable curtailment of solar power, load shedding, and water spillage. Hence, this paper introduces a robust optimization model for HES scheduling. The primary objectives are to enhance the integration of renewable energy sources, mitigate water spillage, minimize peak-valley differences in multiple external grids, and alleviate transmission congestion within the HES-connected grid. To validate the effectiveness of this approach, both a modified IEEE 6-bus system and a real-world case study from the Yalong River region in Southwest China are employed. Numerical results illustrate that by involving the HES in local grid congestion management, a substantial reduction in PV generation curtailment and water wastage is achievable, with minimal impact on peak load management in multiple external grids.

INDEX TERMS Cascade hydropower plants, pumped-storage, renewable energy integration, generation scheduling, peak shaving, multiple interconnected power grids

I. INTRODUCTION

A. MOTIVATION

China has made substantial advancements in the adoption of renewable energy as part of its commitment to reaching peak carbon dioxide emissions by 2030 and achieving carbon neutrality by 2060 [1]. This transformation in China's energy sector is driven by the dual challenges of global climate change and ecological degradation. By 2030, hydropower generation is expected to contribute about 46% of total renewable energy output [2]. Ensuring the sustainable development of the hydropower is of paramount importance for China's energy transition and the attainment of its carbon emission reduction objectives.

Southwest China possesses substantial hydropower potential, amounting to 694,400 MW, with a technically feasible installed capacity of 541,640 MW, making it the world's leader in hydropower capacity [3]. Despite the rapid expansion of hydropower development in the region, the growth in electricity consumption across various southwestern provinces is slow, resulting in a mismatch between installation expansion and market demand [4]. Sluggish demand and limited transmission capacity have hindered hydropower consumption. These challenges stem from complex terrain in water-rich mountainous areas, which requires careful consideration of ecological and environmental impacts in transmission line construction, as well as significant upfront costs for development, population resettlement, and environmental management [5].

Besides, southwest China possesses abundant solar power resources on a significant scale [6]. Many photovoltaic (PV) facilities have been established to harness these pristine energy sources [7]. Solar and hydropower plants together constitute comprehensive renewable power systems in Southwest China. However, the integration of solar power into mountainous regions faces challenges due to limited electrical connectivity to the external grid, potentially leading to performance degradation in hydro-solar hybrid power systems due to solar power fluctuations. The constrained transmission line capacity in the Southwest further impedes the integration of renewable energy resources.

In summary, a disparity exists between the growth of renewable energy installations and the constrained transmission line capacity in Southwest China. Consequently, curtailment of PV generation and water spillage is an inescapable outcome, even as the region grapples with an insufficient electricity supply. To address this challenge, the collaborative dispatching scheme of the hydro/pumped-storage/PV hybrid energy (HES) system presents a promising and cost-effective solution [8].

B. LITERATURE REVIEW

Researchers have explored diverse optimization techniques to enhance the efficiency and performance of cascade hydropower systems. Research [9] presents an ultrashort-term model for optimizing the scheduling of interbasin cascade hydropower plants to meet load demands. Research [10] introduces the multi-objective tangent algorithm (MOTA) to optimize cascade reservoir operation, considering hydropower generation, ecology, and navigation objectives. Research [11] outlines a short-term scheduling strategy for cascade hydropower plants, aiming to identify market opportunities and make optimal market decisions. Research [12] combines simulated annealing with particle swarm optimization to improve the accuracy and efficiency of hourly generation scheduling for cascade hydropower plants with complex hydraulic coupling and head-dependent prohibited operating zones. [13] investigates the impact of climate change on total power generation in cascade hydropower stations. [14] proposes a decentralized monthly generation scheduling model for cascade hydropower plants in multiple time-scale markets. Reference [15] develops optimal bidding strategies for large-scale hydropower stations serving multiple power grids. These studies present various optimization techniques to address long-term generation scheduling challenges in cascade hydropower systems. However, it's essential to note that these reviewed research studies have not extensively explored emerging challenge of integrating renewable energy.

To ensure feasible scheduling and enhance renewable energy utilization, [16] introduces a novel multi-stage robust scheduling method for cascade hydropower systems incorporating uncertainty factors like solar, wind, and natural inflow. Reference [17] offers a model for optimizing wind-solar-hydro hybrid generation systems, leveraging cascade hydropower to address intermittent renewables. [18] suggests adopting linearization methods to model the original hydro-wind-solar hybrid system as a mixed-integer linear programming (MILP) formulation. In research [19], an optimal scheduling model for a complementary hydro-wind-PV-battery system under extreme weather conditions is investigated. [20] addresses multiple power supply risks and the economy of hydropower operation, incorporating more data on renewable energy uncertainties in decision-making to mitigate variability impacts. In research [21], the flexibility of a wind-PV-hydro multi-energy complementary base is assessed, accounting for the compensation capacity of cascade hydropower stations. However, these studies fail to consider the cross-regional power transmission demand, which also hinders the absorption of renewable energy.

Long-distance and large-capacity transmission of hydropower to load centers is essential for accommodating extensive renewables in China [22]. In research [23], a three-stage hybrid method addresses engineering challenges arising from multilateral generation contracts, strong hydraulic-electric relationships, load variations, and spatial-temporal constraints. Reference [24] develops an MILP model to minimize peak-valley differences in multiple grids, resulting in significant reductions in peak loads. Reference [25] minimizes peak-valley differences while considering operational constraints and HVDC tie-lines. Reference [26] integrates peak shaving requirements of receiving-end grids and hydraulic constraints of pumped storage plants. Reference [27] optimizes peak-valley load differences in multiple power grids, considering hydraulic, electrical, and head effect constraints for accurate scheduling. Research [28] addresses accurate modeling and assessment of the value of pumped storage hydropower (PSH) plants in serving the power system. In [29], the authors address safeguarding the sending-end grid's security when multiple hydropower stations share an HVDC transmission channel. Reference [30] explores installing pumped-storage hydro turbines in cascade reservoirs to optimize peak shaving operations, considering hydraulic and unit operation constraints and the impact of water head on unit generation for accurate results. The existing research extensively examines multi-grid peak management via collaboratively dispatching the hydro/pumped-storage/PV hybrid energy system. However, the network constraints within this hybrid energy system are often neglected. This will also cause the PV generation curtailment and water spillage.

C. MAIN CONTRIBUTION

To address the research gap discussed above, this paper presents a mixed-integer linear programming (MILP) model that maximizes the potential of HES to enhance renewable energy utilization and minimize the peak-valley difference across multiple grids, while relieving transmission congestion within the HES-connected grid. Table 1 reveals a comparison of the previous published works with the proposed research.

TABLE 1 COMPARISON BETWEEN THIS STUDY AND PREVIOUS LITERATURE.

References	Optimal generation scheduling	Considering uncertainty of renewables	Participating in multiple grids peak management	Participating in local grid congestion management
[10]-[16]	✓	×	×	×
[17]-[24]	✓	✓	×	×
[25]-[34]	✓	✓	✓	×
This paper	✓	✓	✓	✓

The remaining part of this paper is structured as follows: Section 2 introduces the mathematical formulation for the proposed problem. In Section 3, the simulation results are presented. Finally, Section 4 presents the conclusions drawn from the study.

II. FRAMEWORK FOR ROBUST OPTIMIZATION

Consider the following linear optimization problem

$$\max \boldsymbol{c}^{\mathrm{T}}\boldsymbol{x} \tag{1}$$

$$s.t. \quad \boldsymbol{a}^{\mathrm{T}}\boldsymbol{x} \le \tilde{b} \tag{2}$$

where $\boldsymbol{c}$ and $\boldsymbol{a}$ are n-by-1 vectors of coefficient. n is the number of variables. $\tilde{b}$ is uncertain and can be defined as follows:

$$b = \bar{b} - \boldsymbol{\xi}^{\mathrm{T}}\hat{\boldsymbol{b}} \tag{3}$$

where $\bar{b}$ denotes the nominal value of the coefficient. $\hat{\boldsymbol{b}}$ is a n-by-1 vector of constant variation from the nominal value $\bar{b}$. $\boldsymbol{\xi}$ is a m-by-1 vector of random variables which are subject to an uncertainty set $\mathcal{U}$. m is the number of uncertain variables. One realization of $\mathcal{U}$ can be defined as:

$$\mathcal{U} = \{\boldsymbol{\xi} \mid \boldsymbol{\xi}^{\mathrm{T}}\boldsymbol{e} \le \Gamma, \quad 0 \le \boldsymbol{\xi} \le 1\} \tag{4}$$

where $\boldsymbol{e}$ is a m-by-1 vector whose elements are all equal to one. Γ is a parameter which is known as the uncertainty budget. The value of Γ ranges from 0 to n. $\Gamma = 0$ means that all the parameters are deterministic and the model dose not incorporate uncertainty. $\Gamma = n$ leads to the most conservative case. The objective of robust optimization is to identify solutions that remain feasible for all realizations of the uncertain parameter $\boldsymbol{\xi}$ within the uncertainty set $\mathcal{U}$, thereby providing immunity against infeasibility [35]. Hence, the constraint (2) can be rewritten as:

$$\boldsymbol{a}^{\mathrm{T}}\boldsymbol{x} + \max_{\boldsymbol{\xi}\in\mathcal{U}} \boldsymbol{\xi}^{\mathrm{T}}\hat{\boldsymbol{b}} \le \bar{b} \tag{5}$$

According to dual theory, the maximization problem inside constraint (5) can be reformulated by:

$$\min \Gamma\lambda_{m+1} + \sum_{i=1}^{m}\lambda_i \tag{6}$$

$$s.t. \quad \lambda_i + \lambda_{m+1} \ge \hat{b}_i, \quad \forall i \in m \tag{7}$$

$$\lambda_i \ge 0, \quad \forall i \in m \tag{8}$$

where λ_i is the dual decision variables. $\hat{b}_i$ is the ith element in $\hat{\boldsymbol{b}}$. Incorporating constraints (6)-(8) into (5), we can obtain the linear robust counterpart problem shown as follows:

$$\boldsymbol{a}^{\mathrm{T}}\boldsymbol{x} + \Gamma\lambda_{m+1} + \sum_{i=1}^{m}\lambda_i \le \bar{b} \tag{9}$$

$$s.t. \quad \lambda_i + \lambda_{m+1} \ge \hat{b}_i, \quad \forall i \in m \tag{10}$$

$$\lambda_i \ge 0, \quad \forall i \in m \tag{11}$$

Therefore, the origin robust optimization problem described by (1) and (2) can be reformulated by tractable robust counterpart expressed by (9) to (11).

III. MATHEMATICAL FORMULATION

A. PROBLEM STATEMENT

Fig. 1 illustrates a simplified representation of the hydro/PV/pumped-storage HES along with the grid to which it is connected.

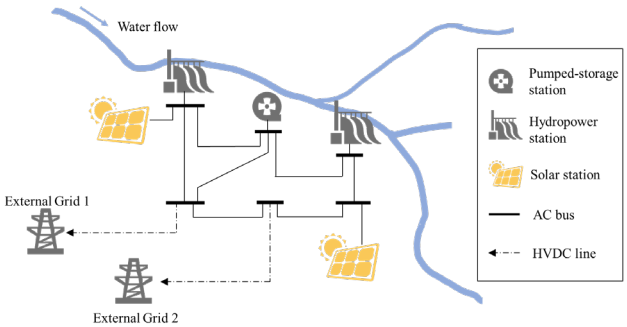

FIGURE 1. **An illustrative system example**

As shown in Fig.1, two hydropower stations and one pumped-storage station are situated in the same runoff area. Each station is connected to distinct alternating current (AC) buses. Additionally, two solar stations contribute active power to two AC buses. Moreover, two high-voltage direct current (HVDC) lines transmit power to two external grids. It can be seen that the integration of renewable energies is influenced by the capacity of transmission lines and the security considerations associated with HVDC lines. Consequently, elaborate adjustments should be made to the power generation of diverse types of power stations. Moreover, the variability and uncertainty of water inflow and PV generation necessitate their inclusion in the scheduling of HES.

B. TRACTABLE ROBUST MODEL FOR OPTIMAL SCHEDULING OF HES

To improve the utilization of the renewable energy, reduce the peak-valley difference of multiple provincial grids, and relieving the transmission congestion within the HES connected grid, this section aims to present the overall objective and constraints of the proposed robust optimization model. Besides, the uncertainties of PV generation and water inflow are also considered in the model.

1) OBJECTIVE FUNCTION

The objective includes the cost of peak-valley difference of multiple external grids, the spilled water, and the curtailed PV generation.

$$f = \min \sum_{n\in\mathcal{N}} \alpha(R_n^{\max} - R_n^{\min}) + \sum_{i\in\mathcal{B}^{\mathrm{H}}}\sum_{t\in\mathcal{T}} c_i^{\mathrm{H}} \Delta P_{i,t}^{\mathrm{H}} + \sum_{i\in\mathcal{B}^{\mathrm{PV}}}\sum_{t\in\mathcal{T}} c_i^{\mathrm{PV}} \Delta P_{i,t}^{\mathrm{PV}} \tag{12}$$

where $\mathcal{N}$ is the set of the external grid numbers. $R_n^{\max}$ and $R_n^{\min}$ are the maximum and minimum residual load of grid n. α is a coefficient indicating the cost of peak-valley difference. $\Delta P_{i,t}^{\mathrm{H}}$ is the equivalent power generated by the spilled water at time interval t. c_i^{H} is the cost of spilled water. $\mathcal{B}^{\mathrm{H}}$ is the set of the buses that connect with a hydropower station. $\mathcal{T}$ is the set of the time intervals. $\Delta P_{i,t}^{\mathrm{PV}}$ is the PV generation curtailment at time interval t. c_i^{PV} is the cost of PV generation curtailment. $\mathcal{B}^{\mathrm{PV}}$ is the set of the buses that connect with a PV power station. $R_n^{\max}$ and $R_n^{\min}$ satisfy:

$$R_n^{\max} = \max\{R_{n,t} \mid t\in\mathcal{T}, n\in\mathcal{N}\} \tag{13}$$

$$R_n^{\min} = \min\{R_{n,t} \mid t\in\mathcal{T}, n\in\mathcal{N}\} \tag{14}$$

where $R_{n,t}$ is the residual load demand of the external grid n at time interval t. The constraints (13) and (14) can be readily tackled by the commercial optimization tools such as CPLEX and GUROBI. For further information, the readers can refer to [26].

2) CASCADE HYDROPOWER CONSTRAINTS

The generation of the hydropower can be approximated by [31]:

$$P_{i,t}^{\mathrm{H}} = 9.81\eta_i Q_{i,t} H_i, \quad \forall t\in\mathcal{T}, \forall i\in\mathcal{B}^{\mathrm{H}} \tag{15}$$

$$\underline{P}_i^{\mathrm{H}} \le P_{i,t}^{\mathrm{H}} \le \overline{P}_i^{\mathrm{H}}, \quad \forall t\in\mathcal{T}, \forall i\in\mathcal{B}^{\mathrm{H}} \tag{16}$$

where $P_{i,t}^{\mathrm{H}}$ denotes the power generation of a specific hydropower plant within a given time interval indexed as t. η_i represents the hydroelectric conversion efficiency of the aforementioned hydropower plant. $Q_{i,t}$ corresponds to the quantity of water flow used for electricity generation at time t, while H_i represents the height of the water head. $\underline{P}_i^{\mathrm{H}}$ and $\overline{P}_i^{\mathrm{H}}$ denote the lower and upper boundaries, respectively, of the power generation for the hydropower plant i. The water balance constraints for the cascade hydropower stations in the same runoff are shown in [17]:

$$C_{i,t}^{\mathrm{H}} = C_{i,t-1}^{\mathrm{H}} + 3600[J_{i,t} - (Q_{i,t} + V_{i,t})], \ \forall t\in\mathcal{T}, \forall i\in\mathcal{B}^{\mathrm{H}} \tag{17}$$

$$J_{i,t} = Q_{\alpha(i),t-\tau} + V_{\alpha(i),t-\tau} + W_{i,t}, \ \forall t\in\mathcal{T}, \forall i\in\mathcal{B}^{\mathrm{H}} \tag{18}$$

where $C_{i,t}^{\mathrm{H}}$ and $C_{i,t-1}^{\mathrm{H}}$ denote the reservoir capacity at time t and $t-1$. $V_{i,t}$ is the spilled water at time t. Δt is the length of time intervals. $J_{i,t}$ is the total inflow of the reservoir at the hydropower station that is connected with bus i. $Q_{\alpha(i),t-\tau}$ represents the amount of water utilized for electricity generation at the nearby hydropower station located upstream. $V_{\alpha(i),t-\tau}$ is the amount of spilled water at the nearby hydropower station located upstream. $W_{i,t}$ denotes the incoming volume of natural water at hydropower station at bus i. τ denotes the water flow delay. $C_{i,t}^{\mathrm{H}}$, $Q_{i,t}$, and $V_{i,t}$ are restrained by:

$$\underline{C}_i^{\mathrm{H}} \le C_{i,t}^{\mathrm{H}} \le \overline{C}_i^{\mathrm{H}}, \quad \forall t\in\mathcal{T}, \forall i\in\mathcal{B}^{\mathrm{H}} \tag{19}$$

$$\underline{Q}_i \le Q_{i,t} + V_{i,t} \le \overline{Q}_i, \quad \forall t\in\mathcal{T}, \forall i\in\mathcal{B}^{\mathrm{H}} \tag{20}$$

where $\underline{C}_i^{\mathrm{H}}$ and $\overline{C}_i^{\mathrm{H}}$ are the lower and upper limits of the reservoir capacity, respectively. $\underline{Q}_i$ and $\overline{Q}_i$ are the minimum and the maximum water flow rate.

In practice, the natural water inflow $W_{i,t}$ are uncertain, which is intractable in the scheduling of the HES [32]. To capture the uncertain nature of water inflow, $W_{i,t}$ can be expressed by [33]:

$$W_{i,t} = \hat{W}_{i,t} + \xi_{i,t}^{+}\overline{W}_{i,t} - \xi_{i,t}^{-}\underline{W}_{i,t}, \forall t\in\mathcal{T}, \forall i\in\mathcal{B}^{\mathrm{H}} \tag{21}$$

where $\hat{W}_{i,t}$ denotes the predicted natural water inflow. $\overline{W}_{i,t}$ and $\underline{W}_{i,t}$ are the maximum and minimum deviations of the water inflow. $\xi_{i,t}^{+}$, and $\xi_{i,t}^{-}$ are the coefficients which reflect the tolerable range for the uncertainty [34]. The uncertainty set $\mathcal{U}^{\xi}$ can be defined as:

$$\xi_{i,t}^{+} + \xi_{i,t}^{-} \le \tau^{\xi}, \quad \tau^{\xi}\in[0,2] \tag{22}$$

$$0 \le \xi_{i,t}^{+}, \xi_{i,t}^{-} \le 1 \tag{23}$$

where τ^{ξ} denotes the uncertainty budget which is used to adjust the ranges of uncertainty. According to (17)-(19), we can derive the tractable robust counterpart using the method discussed in Section II.

$$\lambda_1 + \lambda_2 + \tau^{\xi}\lambda_3 \le \left(\frac{\overline{C}_i^{\mathrm{H}} - C_{i,t-1}^{\mathrm{H}}}{3600} + Q_{i,t} + V_{i,t} - Q_{\alpha(i),t-\tau} - V_{\alpha(i),t-\tau} - \hat{W}_{i,t}\right) \tag{24}$$

$$\lambda_1 + \lambda_3 \ge \overline{W}_{i,t} \tag{25}$$

$$\lambda_2 + \lambda_3 \ge -\underline{W}_{i,t} \tag{26}$$

$$\lambda_1, \lambda_2, \lambda_3 \ge 0 \tag{27}$$

where λ_1, λ_2, and λ_3 are the dual variables of the corresponding constraints in the uncertainty set $\mathcal{U}$.

3) PUMPED-STORAGE OPERATING CONSTRAINTS

The charging and discharging power of a pumped-storage power station are limited by [31]:

$$u_{i,t}^{\mathrm{c}}\underline{P}_{i,t}^{\mathrm{c}} \le P_{i,t}^{\mathrm{c}} \le u_{i,t}^{\mathrm{c}}\overline{P}_{i,t}^{\mathrm{c}}, \quad \forall t\in\mathcal{T}, \forall i\in\mathcal{B}^{\mathrm{P}} \tag{28}$$

$$u_{i,t}^{\mathrm{d}}\underline{P}_{i,t}^{\mathrm{d}} \le P_{i,t}^{\mathrm{d}} \le u_{i,t}^{\mathrm{d}}\overline{P}_{i,t}^{\mathrm{d}}, \quad \forall t \in \mathcal{T}, \forall i \in \mathcal{B}^{\mathrm{P}} \tag{29}$$

$$u_{i,t}^{\mathrm{c}} + u_{i,t}^{\mathrm{d}} \le 1, \quad \forall t \in \mathcal{T}, \forall i \in \mathcal{B}^{\mathrm{P}} \tag{30}$$

where $P_{i,t}^{\mathrm{c}}$ and $P_{i,t}^{\mathrm{d}}$ are the charging and discharging power, respectively, of the pumped-storage station that connects with the bus i at the time interval t. $\underline{P}_{i,t}^{\mathrm{c}}$ and $\overline{P}_{i,t}^{\mathrm{c}}$ are the lower and upper boundaries, respectively, of the charging power. $\underline{P}_{i,t}^{\mathrm{d}}$ and $\overline{P}_{i,t}^{\mathrm{d}}$ are the range of discharge power. $u_{i,t}^{\mathrm{c}}$ indicates the charging state of the pumped-storage station and $u_{i,t}^{\mathrm{d}}$ indicates the discharging state. $\mathcal{B}^{\mathrm{P}}$ is the set of the buses that connect with pumped-storage station. (31) imposes a restriction on the pumped-storage station, preventing it from simultaneously being in both the charging and discharging states. The constraint for reservoir capacity of a pumped-storage power station is represented as:

$$C_{i,t}^{\mathrm{p}} = C_{i,t-1}^{\mathrm{p}} + u_{i,t}^{\mathrm{c}}P_{i,t}^{\mathrm{c}}\eta^{\mathrm{c}} - u_{i,t}^{\mathrm{d}}P_{i,t}^{\mathrm{d}}\eta^{\mathrm{d}} \tag{31}$$

$$\underline{C}_{i}^{\mathrm{p}} \le C_{i,t}^{\mathrm{p}} \le \overline{C}_{i}^{\mathrm{p}} \tag{32}$$

where $C_{i,t}^{\mathrm{p}}$ represents the reservoir capacity of the pumped-storage power station that connects with the bus i. The lower and upper bounds of the reservoir capacity are represented by $\underline{C}_{i}^{\mathrm{p}}$ and $\overline{C}_{i}^{\mathrm{p}}$, respectively. Furthermore, the coefficient η^{c} signifies the conversion ratio of electricity to water, while the coefficient η^{d} represents the conversion ratio of water back to electricity.

4) HVDC CONSTRAINTS

To ensure the safe operation, the power through HVDC lines should satisfy [29]:

$$\underline{P}_{l}^{\mathrm{HVDC}} \le P_{l,t}^{\mathrm{HVDC}} \le \overline{P}_{l}^{\mathrm{HVDC}} \tag{33}$$

$$\left|P_{l,t}^{\mathrm{HVDC}} - P_{l,t-1}^{\mathrm{HVDC}}\right| \le \Delta P_{l}^{\mathrm{HVDC}} \tag{34}$$

where $P_{l,t}^{\mathrm{HVDC}}$ represents the power transmitted through HVDC line l at a specific time t, constrained by the upper limit $\overline{P}_{l}^{\mathrm{HVDC}}$ and lower limit $\underline{P}_{l}^{\mathrm{HVDC}}$. $\Delta P_{l}^{\mathrm{HVDC}}$ is the maximum ramping rate of the power in HVDC lines.

5) NETWORK CONSTRAINTS

The network constraints mainly include the power balance constraints and the line flow limitations.

$$P_{i,t}^{\mathrm{H}} + P_{i,t}^{\mathrm{PV}} + P_{i,t}^{\mathrm{d}} - P_{i,t}^{\mathrm{c}} - P_{i,t}^{\mathrm{L}} = \sum_{j \in i} P_{ij,t} + P_{l,t}^{\mathrm{HVDC}} \tag{35}$$

$$P_{ij,t} = b_{ij}(\theta_{i,t} - \theta_{j,t}) \tag{36}$$

$$\underline{P}_{ij} \le P_{ij,t} \le \overline{P}_{ij} \tag{37}$$

$$P_{i,t}^{\mathrm{PV}} \le \tilde{P}_{i,t}^{\mathrm{PV}}(\boldsymbol{\epsilon}) \tag{38}$$

where $P_{i,t}^{\mathrm{L}}$ is the load demand at the bus i during the time interval t. $P_{ij,t}$ is the power flow in line i-j. $\theta_{i,t}$ denotes the phase angle at bus i. $\underline{P}_{ij}$ and $\overline{P}_{ij}$ are the lower and upper limits, respectively, of the power flow in line i-j. $\tilde{P}_{i,t}^{\mathrm{PV}}(\boldsymbol{\epsilon})$ is the available PV output which is determined by $\boldsymbol{\epsilon}$ as shown in:

$$\tilde{P}_{i,t}^{\mathrm{PV}}(\boldsymbol{\epsilon}) = \hat{P}_{i,t}^{\mathrm{PV}} + \epsilon^{+}\overline{P}_{i,t}^{\mathrm{PV}} - \epsilon^{-}\underline{P}_{i,t}^{\mathrm{PV}} \tag{39}$$

where $\overline{P}_{i,t}^{\mathrm{PV}}$ and $\underline{P}_{i,t}^{\mathrm{PV}}$ are the maximum and minimum deviations of the PV output. $\epsilon_{i,t}^{+}$ and $\epsilon_{i,t}^{-}$ are the coefficients which reflect the tolerable range for the uncertainty. $\boldsymbol{\epsilon}$ is defined on the uncertainty set $\mathcal{U}^{\epsilon}$ which is described as:

$$0 \le \epsilon^{+}, \epsilon^{-} \le 1 \tag{40}$$

$$\epsilon^{+} + \epsilon^{-} \le \tau^{\epsilon}, \quad \tau^{\epsilon} \in [0,2] \tag{41}$$

where τ^{ϵ} denotes the uncertainty budget which is used to adjust the ranges of uncertainty. Similarly, the robust counterpart constraint of (39) can be formulated as:

$$\zeta_1 + \zeta_2 + \tau^{\epsilon}\zeta_3 \le \hat{P}_{i,t}^{\mathrm{PV}} - P_{i,t}^{\mathrm{PV}} \tag{42}$$

$$\zeta_1 + \zeta_3 \ge -\overline{P}_{i,t}^{\mathrm{PV}} \tag{43}$$

$$\zeta_1 + \zeta_2 \ge \underline{P}_{i,t}^{\mathrm{PV}} \tag{44}$$

$$\zeta_1, \zeta_2, \zeta_3 \ge 0 \tag{45}$$

where ζ_1, ζ_2, and ζ_3 are the dual variables of the corresponding constraints.

6) EXTERNAL GRID POWER RECEIVING CONSTRAINTS

As mentioned above, the external grids can receive power through HVDC lines. Nevertheless, due to the technical considerations, there exists a limit on the total power that an external grid can receive. Hence, the amount of power received by an external grid is subject to constraints defined by the subsequent expressions [23].

$$R_{n,t} = P_{n,t} - \sum_{l \in n} P_{l,t}^{\mathrm{HVDC}} \tag{46}$$

$$\sum_{t \in \mathcal{T}} \sum_{l \in n} P_{l,t}^{\mathrm{HVDC}} \le E_{n}^{\max} \tag{47}$$

where $R_{n,t}$ is the residual load of the external grid n at time t. $P_{n,t}$ is the initial load of the external grid n at time t. $l \in n$ means the HVDC line l connects with the external grid n. $E_{n}^{\max}$ denotes the maximum amount of power the external grid n can receive throughout a day.

To summarize, the proposed model for optimal scheduling of the HES is formulated as follows:

$$\begin{aligned} &\min \ f \\ &s.t. \quad \{(13)\text{-}(16),\ (20),\ (25)\text{-}(38),\ (43)\text{-}(48)\} \end{aligned} \tag{48}$$

Model (49) is entirely a MILP model. It can be solved straightforward using the GUROBI solver [37, 38].

IV. CASE STUDY

To demonstrate the benefits of this method, it is applied to a modified IEEE 6-bus test system and a real-world case extracted from the Yalong River in Southwest China. Subsequent sections will discuss the simulation results.

A. A MODIFIED IEEE 6-BUS TEST SYSTEM

1) SIMULATION SETUP

The system configuration is shown in Fig. 1 where two hydropower stations locate at bus 1 and 3, one pumped-storage station situates at bus 2, and two solar stations position at bus 1 and 6. Additionally, two HVDC lines link two external grids. The parameters of the hydropower station and pumped-storage station are detailed in TABLE II and III, respectively. Due to the lack of real-world data, all the parameters that exhibits in TABLE II and III are assumed based on [11] and [38].

TABLE II PARAMETERS OF HYDROPOWER STATION

Bus	$\overline{C}_h^{\mathrm{H}} \setminus \underline{C}_h^{\mathrm{H}}$ ($\times 10^7 \mathrm{m}^3$)	Capacity (MW)	$\overline{Q}_h \setminus \underline{Q}_h$ (m^3/s)	η_h (%)	Ramping rate (MW)
1	[1, 5]	800	[200, 1700]	89	200
3	[3, 10]	1000	[200, 1500]	80	250

TABLE III PARAMETERS OF PUMPED-STORAGE STATION

Bus	$\overline{C}_h^{\mathrm{p}} \setminus \underline{C}_h^{\mathrm{p}}$ ($\times 10^7 \mathrm{m}^3$)	Capacity (MW)	η^{c} (%)	η^{d} (%)	Ramping rate (MW)
2	[2, 6]	200	95	95	50

Additionally, the capacity of the two HVDC lines is 800MW with $\Delta P_l^{\mathrm{HVDC}}$ equals 200MW. The installation capacities of the two PV station are 400MW and 300MW, respectively. The PV generation and water inflow throughout a day are shown in Figs. 2 and 3, respectively.

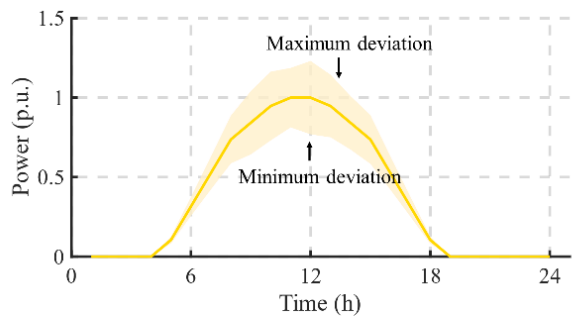

FIGURE 2. **Hourly PV generation during a typical day**

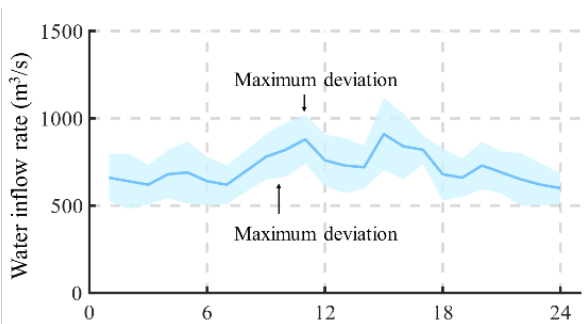

FIGURE 3. **Hourly natural water inflow rate during a typical day**

2) INITIAL SYSTEM STATES

The initial curtailed PV generation and the spilled water are depicted in Figs. 4 and 5.

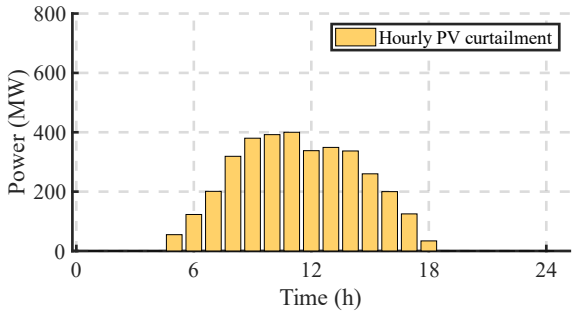

FIGURE 4. **Initial curtailed PV generation.**

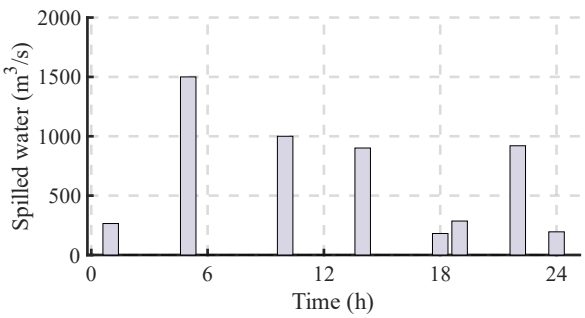

FIGURE 5. **Initial spilled water.**

According to Figs. 4 and 5, the cumulative PV generation curtailment amounts to 3445.9MWh over the course of a day, while the total volume of spilled water reaches 5342.4m^3. The initial line load ratio is presented in Fig 6.

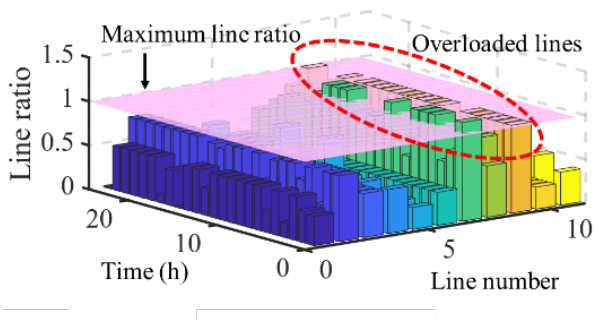

FIGURE 6. **Initial line load ratio.**

As shown in Fig. 6, the plane indicates the maximum line load ratio. Each bar indicates the load ratio of a line. The bars that surpass the plane means these lines are overloaded. It is evident from the figure that two lines, specifically line 7 and line 9, highlighted by red circles, experience overload conditions. Line 7 is overloaded at times 1, 4, 5, 6, 8, 13, 14, and 15 with a maximum line load ratio of 112.5%. Line 9 exhibits overloads during times 1-6, 11-18, 20, and 24, with the maximum line load ratio reaching 103.6%.

3) OPTIMIZATION RESULTS

Applying the proposed MILP model to optimize the modified IEEE 6-bus test system, the results are shown as follows.

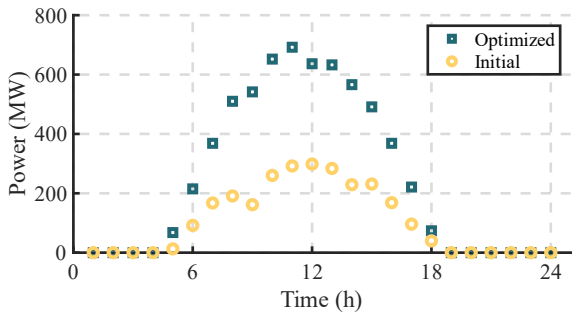

FIGURE 7. **Comparison of the PV generation before and after optimization.**

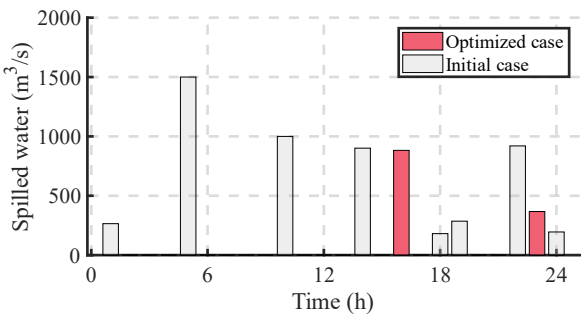

FIGURE 8. **Comparison of the spilled water before and after optimization.**

Based on the data illustrated in Fig. 7, a substantial enhancement is observed in the PV generation. The total accumulated PV generation throughout the day escalates from 2781.5MWh to 6036.4MWh. Furthermore, Fig. 8 demonstrates a reduction in the total volume of spilled water, which diminishes from 5342.4m^3/s to 1249.7m^3/s. The optimized line load ratio is presented in Fig. 9.

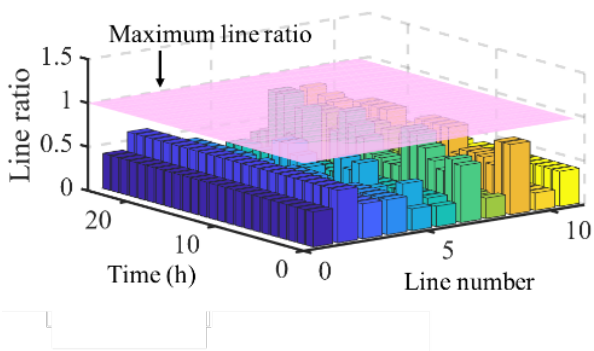

FIGURE 9. **Optimized line ratio.**

In Fig. 9, the two previously overloaded lines have returned to the normal range after optimization. All the bars now fall below the maximum line ratio plane, indicating the absence of overloaded lines. The proposed model has effectively relieved transmission congestion within the HES-connected grid. The residual load for each external grid is illustrated in Figs. 10 and 11.

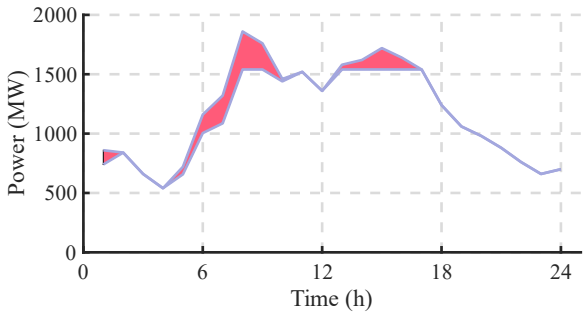

FIGURE 10. **Residual load of the external grid 1.**

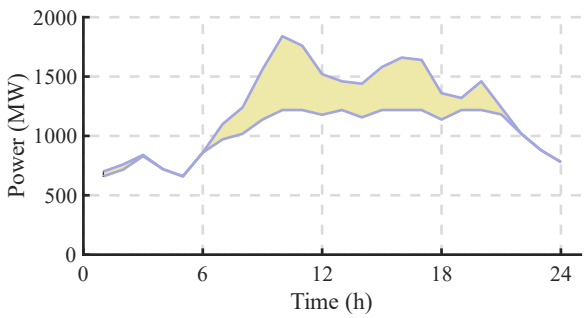

FIGURE 11. **Residual load of the external grid 2.**

As it is presented in Fig. 10, the peak-valley difference of external grid one undergoes a reduction from 1320MW to 1000MW, reflecting a decrease of 24.24% in the initial peak-valley difference. Similarly, the peak-valley difference of external grid 2 diminishes from 1180MW to 558.07MW, resulting in a reduction of 52.71% in the initial peak-valley difference of external grid 2. The power through HVDC lines is shown in Fig. 12.

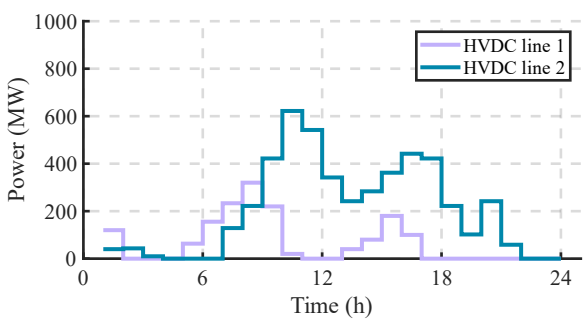

FIGURE 12. **Power through two HVDC lines**

From Fig. 12, it is evident that the active power transmitted via HVDC Line 1 increases from 6:00 to 8:00 and 13:00 to 15:00, while it decreases from 9:00 to 10:00 and 16:00 to 18:00. This contributes to the mitigation of the first peak load at 8:00 and the second peak load at 15:00 in External Grid 1. In the case of HVDC Line 2, the active power rises from 7:00 to 11:00 and 14:00 to 16:00, but decreases from 11:00 to 13:00 and 17:00 to 19:00. This helps in managing the first peak load

at 8:00 and the second peak load at 15:00 in External Grid 2. The cumulative power supply for External Grid 1 and Grid 2 amounts to 1532.1MWh and 4747.4MWh, respectively. As shown in Figs. 10 and 11, the performance of peak shaving achieved by Grid 1 is inferior to that of Grid 2. One possible explanation is the constrained line capacity that hampers power transmission to External Grid 1 via HVDC Line 1.

The optimal scheduling of the two cascade hydropower stations and one pumped-storage station is shown in Figs. 13-15.

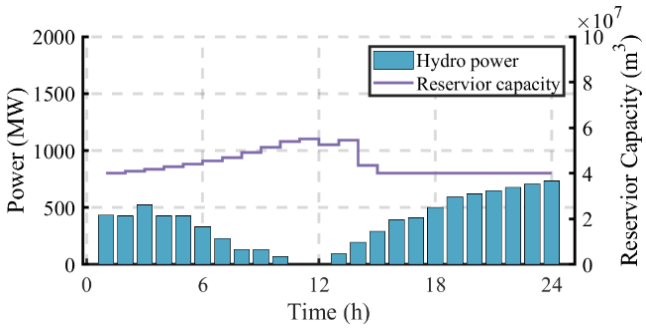

FIGURE 13. **Optimized power generation of the hydropower 1.**

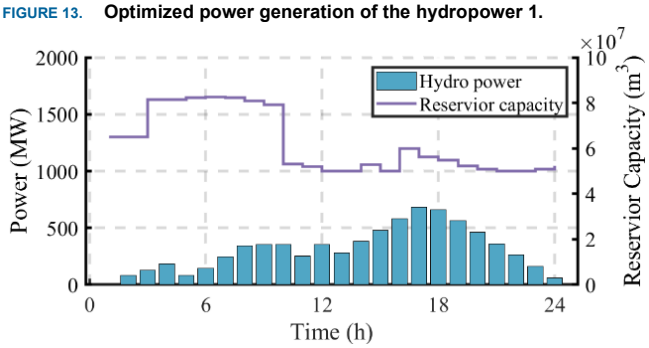

FIGURE 14. **Optimized power generation of the hydropower 2.**

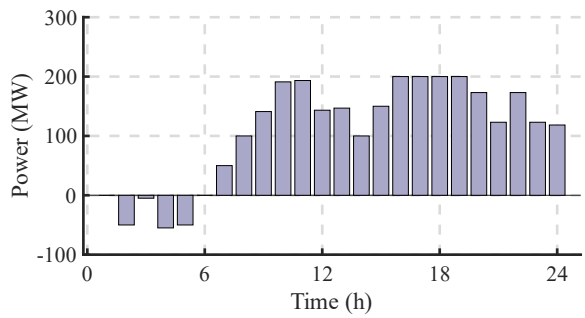

FIGURE 15. **Optimized power generation of the pumped-storage.**

Fig. 13 illustrates a noteworthy trend in the output of hydropower station 1. It steadily decreases from 5:00 to 10:00, coinciding with increased PV generation. Conversely, from 11:00 to 19:00, the output gradually rises as PV generation diminishes. The volume in the reservoir of hydropower station 1 increases during 00:00 to 12:00 and decreases during 13:00 to 24:00. Similarly, hydropower station 2's reservoir volume rises during 00:00 to 6:00 and 12:00 to 17:00, and falls during 7:00 to 11:00 and 17:00 to 24:00. This synchronization between hydropower and PV generation significantly enhances PV integration and reduces water spillage. In Fig. 14, hydropower station 2 exhibits a bimodal output pattern with peaks at 10:00 and 16:00, effectively aiding peak load regulation for the two external grids. As seen in Fig. 15, the pumped-storage station primarily charges from 3:00 to 7:00, preventing water wastage. From 12:00 to 24:00, it gradually discharges power, contributing to peak load regulation for both external grids.

4) A COMPARISON WITH THE PREVIOUS WORKS

To demonstrate the merits of the proposed method, a comparison with the model that only addresses the multiple grids peak management is conducted. To build the model without transmission congestion, we omitted constraints (37) and (38) from the proposed model. The results are shown as follows.

TABLE IV COMPARISON WITH THE PREVIOUS WORKS

Performances	Only consider multiple grid peak management	This paper
Peak-valley differences of external provincial grids	Grid 1: 953.33MW Grid 2: 810MW	Grid 1:1000MW Grid 2: 858.07MW
Load curtailment	834.4090MWh	0MWh
PV generation curtailment	3212.0877MWh	1610.5263MWh
Spilled water	3023.7040m^3/s	1249.7m^3/s

As it is shown in TABLE IV, the peak-valley differences of the two external provincial grids obtained by the previous works that only consider the multiple grid peak management are 953.33MW and 810MW. However, 834.4090MWh local load and 3212.0877MWh PV generation are curtailed. There are also 3023.7040m^3/s water are spilled. In this paper, the peak-valley difference slightly increases by 4.9% in grid 1 and by 5.9% in grid 2 compared with the method that only considers the multiple grid peak management. However, the load curtailment reduces from 834.4090MWh to zero. The curtailment of PV generation reduces from 3212.0877MWh to 1610.5263MWh. The spilled water reduces from 3023.7040m^3/s to 1249.7m^3/s. The results demonstrate that the participation in the local grid congestion management when scheduling the hydropower/PV/pumped-storage HES, the local grid load curtailment can be avoided and the utilization of PV and hydropower can be significantly improved, though it slightly affects the performance of multiple grid peak management.

5) A COMPARISON WITH THE DETERMINISTIC MODEL

As discussed above, the parameters τ^{ξ} and τ^{ϵ} serve to calibrate uncertainty. When both τ^{ξ} and τ^{ϵ} are set to zero, the proposed model is a completely deterministic model. In the subsequent section, various values of τ^{ξ} and τ^{ϵ} are employed to assess the model's performance, with results presented below.

TABLE V COMPARISON WITH THE DETERMINISTIC MODEL

Uncertainty budget	Peak-valley difference (MW)	Curtailed solar energy (MWh)	Curtailed load (MWh)	Spilled water (m^3/s)
$\tau^{\xi}=\tau^{\epsilon}=2$	Grid 1: 1000 Grid 2: 858.07	1610.53	0	1249.7
$\tau^{\xi}=\tau^{\epsilon}=1$	Grid 1: 991.859 Grid 2: 822.8472	805.26	0	1033.2
$\tau^{\xi}=\tau^{\epsilon}=0$	Grid 1: 972.9386 Grid 2: 821.78	0	0	0

TABLE V shows the peak-valley difference, PV generation curtailment, local load curtailment, and water spillage under different uncertainty budget τ^{ξ} and τ^{ϵ}. From table 5, one can observe that as τ^{ξ} and τ^{ϵ} rise from 0 to 2, there is a notable increase in peak-valley differences across multiple grids, PV generation curtailment, and water spillage. This trend primarily stems from the elevated τ^{ξ} and τ^{ϵ} values, which subsequently reduce the estimated available PV power and water inflows for electricity generation, consequently leading to increased PV generation curtailment and water spillage. Furthermore, this diminished PV generation and hydropower supply also affects the performance of managing peak loads across multiple grids.

B. A REAL-WORLD TEST CASE

1) SIMULATION SETUP

To further demonstrate the efficacy of the proposed methodology, a real-world test case abstracted from Yalong River in Southwest China [20] is employed. The system configuration is visualized in Fig. 16.

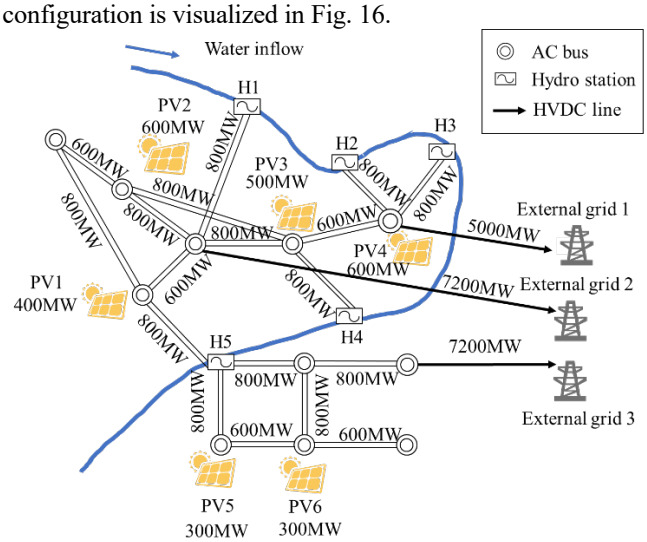

FIGURE 16. System configuration of the real-world test case

As shown in Fig. 16, the test system consists a total of 16 AC buses interconnected by 18 transmission lines. Within this system, five buses are equipped with hydropower stations, while an additional six buses are equipped with solar stations. Moreover, three HVDC lines connect with three external grids, supporting powers to regulate peak management for these three external grids. The parameters of the 5 hydropower stations are detailed in TABLE VI. The PV generation and the water inflow can be referred to Figs. 2 and 3, respectively.

TABLE VI PARAMETERS OF THE HYDROPOWER STATIONS

No.	$\overline{C}_h^{\mathrm{H}} \setminus \underline{C}_h^{\mathrm{H}}$ ($\times 10^6 m^3$)	Capacity (MW)	$\overline{Q}_h \setminus \underline{Q}_h$ (m^3/s)	η_h (%)	Ramping rate (MW)
H1	[1, 5]	1500	[500, 4250]	89	300
H2	[3, 10]	4800	[500, 3750]	89	600
H3	[1, 3]	3000	[500, 4000]	80	500
H4	[3, 8]	2400	[500, 4500]	80	400
H5	[2, 6]	3300	[500, 3750]	80	450

2) INITIAL SYSTEM STATES

The initial curtailment of PV generation and spilled water are depicted in Figs. 17 and 18.

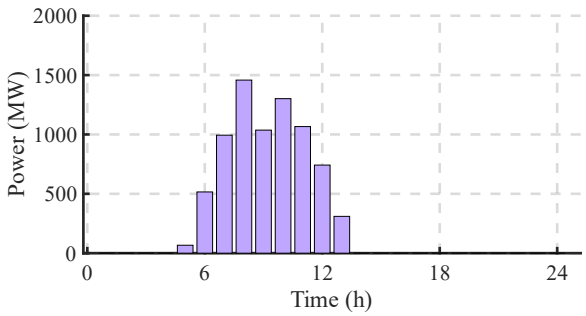

FIGURE 17. Initial PV generation curtailment

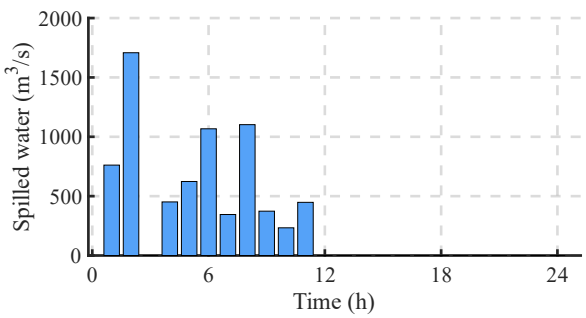

FIGURE 18. Initial amounts of spilled water.

From Fig. 17, it can be observed that the PV generation curtailment occurs during 5:00 to 13:00. The total curtailed PV generation accumulates to 7491.2MWh. Similarly, Fig. 18 illustrates a substantial abandonment of surplus water, peaking at $1708 m^3/s$ at 2:00. This excessive water spillage occurs during a period of relatively low load demand, resulting in a significant volume of wasted water. Additionally, from 5:00 to 11:00, water spillage is also necessary to absorb the excess PV generation. The initial line load ratio is depicted in Fig. 19.

As shown in Fig. 19, it is evident that multiple bars exceed the maximum line ratio plane, indicating that lines 2, 3, 5, 7, 10, and 18 encounter periods of overload during specific time intervals within the given day. The maximum line load ratio reaches 106.7%.

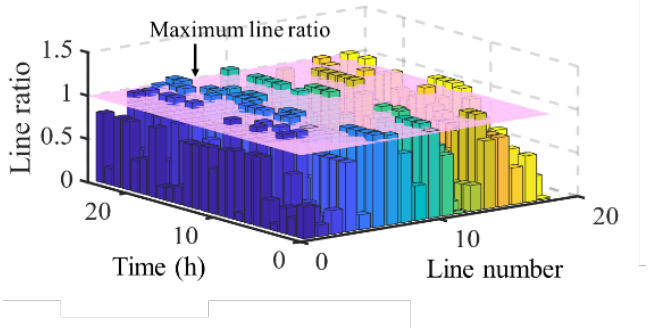

FIGURE 19. **Initial line load ratio**

3) OPTIMIZATION RESULTS

Applying the proposed method to optimize this system, the comparison of PV generation, spilled water and line load ratio are shown in Figs. 20-22.

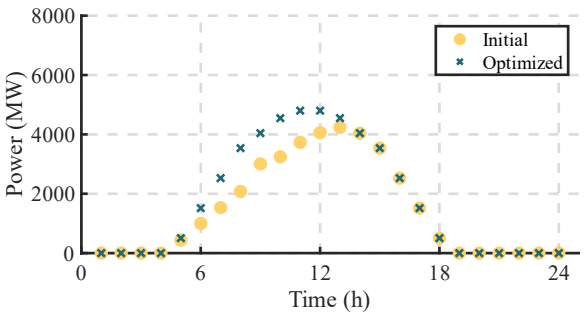

FIGURE 20. **Comparison of PV generation.**

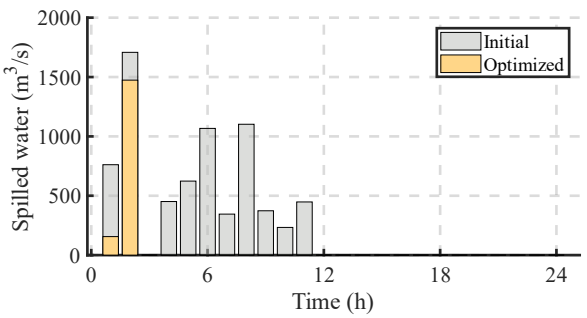

FIGURE 21. **Comparison of spilled water.**

As shown in Fig. 20, the total PV generation increases from 35456MWh to 42947MWh. Additionally, Fig. 21 reveals a reduction in water spillage at 1:00, decreasing from 761.5m3/s to 156m3/s, while the water spillage at 2:00 declines from 1708m3/s to 1473.9m3/s. In other time intervals, all available water resources are effectively utilized. In Fig. 22, the six overload lines have been successfully restored to the normal operating range after optimization. The comparison of peak-valley difference of the three external grids are detailed in TABLE VII.

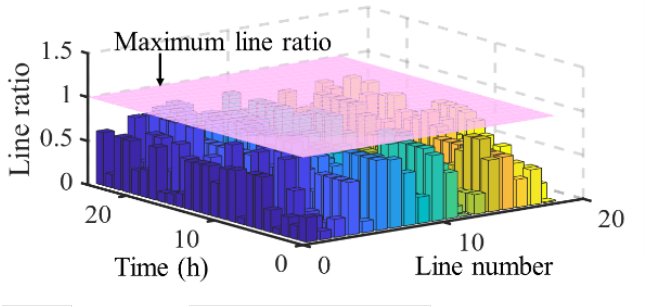

FIGURE 22. **Line load ratio after optimization**

TABLE VII OPTIMIZATION RESULTS OF THE PEAK-VALLEY DIFFERENCE

No.	Initial Peak-valley difference (MW)	Optimized Peak-valley difference (MW)	Percentage (%)
Grid 1	13200	12400	-6.06%
Grid 2	11800	10800	-8.47%
Grid 3	15455	13455	-12.94%

According to the data provided in TABLE VII, the peak-valley difference of external grid 1 experiences a decrease from 13200MW to 12400MW. Similarly, the peak-valley difference of external grid 2 decreases from 11800MW to 10800MW, while the peak-valley difference of external grid 3 is reduced from 15455MW to 12400MW. The power through HVDC lines is shown in Fig. 23.

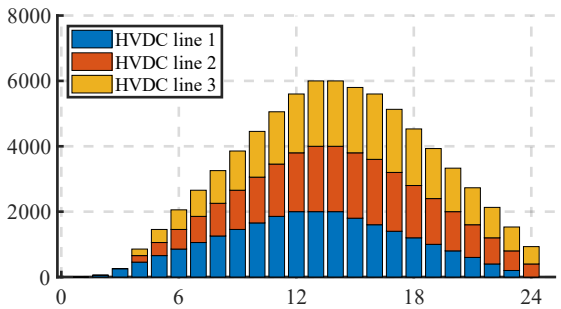

FIGURE 23. **Power through three HVDC lines during the given day**

Fig. 23 illustrates a gradual increase in power transmitted through the three HVDC lines from 3:00 to 14:00, reaching a peak total of 6000MW at 14:00. Subsequently, from 15:00 to 24:00, the power transmitted through the HVDC lines gradually decreases. These results demonstrate that significant reductions in the peak-valley difference of the external grids can be attained by judiciously adjusting the power flow through the HVDC lines. Fig. 24 displays the optimal operating strategy of the cascade hydropower station.

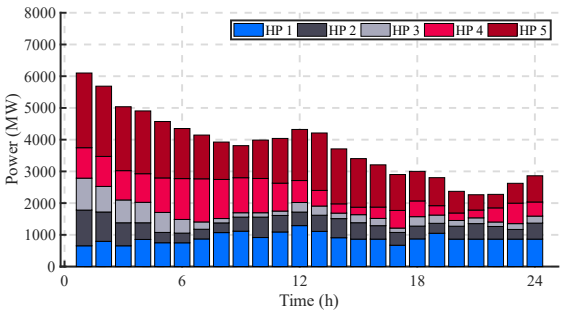

FIGURE 24. Optimal operating strategy of 5 hydropower stations.

In Fig. 24, it is evident that the cumulative generation of the five hydropower sources declines from 1:00 to 9:00 and 12:00 to 16:00, resulting in a 7491MWh increase in PV generation. From 9:00 to 12:00, the total generation of the five hydropower plants increases to support peak load management across the three external grids. This leads to a reduction of the peak-valley difference in the three external grids by 6.06%, 8.47%, and 12.94%, respectively. These outcomes provide compelling evidence that the proposed optimization model is effective in managing peak loads and promoting PV generation.

4) A COMPARISON WITH THE PREVIOUS WORKS

We also compared the proposed method with the previous works using the real-world test case. The results are shown as follows.

TABLE VIII COMPARISON WITH THE PREVIOUS WORKS

Performances	Only consider multiple grid peak management	This paper
Peak-valley differences of external provincial grids	Grid 1: 11200MW Grid 2: 9800MW Grid 3: 13545.55	Grid 1:12400MW Grid 2: 10800MW Grid 3: 13545.55MW
Load curtailment	0MWh	0MWh
PV generation curtailment	6775.70Wh	4294.7368MWh
Spilled water	2282.15m^3/s	1629.9m^3/s

As it is shown in TABLE VIII the peak-valley differences of the three external provincial grids obtained by the previous works that only consider the multiple grid peak management are 11200MW, 9800MW, and 13545.55MW, respectively. However, 6775.70MWh PV generation are curtailed and 3023.7040m^3/s water are spilled. In this paper, the peak-valley difference across the three external grids slightly increases by 10.71%, 10.20%, and 0%, respectively, compared with the method that only considers the multiple grid peak management. However, the PV generation curtailment reduces by 36.62% from 6775.70.4090MWh to 4294.7368MWh. The water spillage reduces by 28.58% from 2282.15m^3/s to 1629.9m^3/s. These results further underscore the advantages of engaging in local grid congestion management when scheduling the hydropower/PV/pumped-storage HES, as it significantly enhances the utilization of PV and hydropower.

5) A COMPARISON WITH THE DETERMINISTIC MODEL

We also compared the results under different uncertainty budgets τ^{ξ} and τ^{ϵ}. The results are shown as follows.

TABLE IX COMPARISON WITH THE DETERMINISTIC MODEL

Uncertainty budget	Peak-valley difference (MW)	Curtailed solar energy (MWh)	Curtailed load (MWh)	Spilled water (m^3/s)
$\tau^{\xi}=\tau^{\epsilon}=2$	Grid 1: 12400 Grid 2: 10800 Grid 3: 13545.55	4294.74	0	1629.9
$\tau^{\xi}=\tau^{\epsilon}=1$	Grid 1: 11300 Grid 2: 10238.303 Grid 3: 12000	4088.60	0	1412.3
$\tau^{\xi}=\tau^{\epsilon}=0$	Grid 1: 11242.14 Grid 2: 10203.02 Grid 3: 12000	1624.07	0	1416.9

From TABLE IX, it is evident that an increase in the values of parameters τ^{ξ} and τ^{ϵ} correlates with heightened peak-valley differences, greater PV generation curtailment, and increased water spillage. When both τ^{ξ} and τ^{ϵ} equal zero, the model transforms into a completely deterministic one. This implies that the available PV power and water inflow match their predicted values, introducing no uncertainty. Although this scenario results in the smallest peak-valley differences, PV generation curtailment, and water spillage, it represents an idealized case for scheduling the hydro/PV/pumped-storage HES, as the possibility of the available PV power and water inflow equal their forecasted values is low. Conversely, when τ^{ξ} and τ^{ϵ} both equal two, the deviations in available PV power and water inflow are larger, leading to reduced solar power integration and increased water spillage. Therefore, $\tau^{\xi}=\tau^{\epsilon}$ can be regarded as the most conservative scheduling plan for the hydropower/PV/pumped-storage HES.

V. CONCLUSION

In this paper, a tractable robust optimization model for optimizing hydro/pumped-storage/PV HES is developed. The aim of the proposed model is to enhance the integration of renewable energy sources, reduce water spillage, and alleviate peak-valley differences in various external grids while considering the network constraints within the HES. Numerical results, based on a real-world test case extracted from the Yalong River region in Southwest China, demonstrate that by finely adjusting HES output while considering network constraints, solar power utilization increases by 21.14%, and water spillage decreases by 34%. The peak-valley differences in three external grids decrease by 6.06%, 8.47%, and 12.94%, respectively. Compared to the previous works, the proposed method significantly reduces the PV generation curtailment, water spillage, and the peak-valley

differences of multiple-grids while relieving the transmission congestion within the HES-connected grid.

Future research can be extended in three key areas. Firstly, considering that robust optimization methods tend to be conservative, exploring the potential of distributionally robust optimization in HES scheduling is valuable. Secondly, to enable voltage regulation, integrating AC power flow constraints into the model presents a promising avenue. Thirdly, given the increasing frequency of extreme weather events, it becomes imperative to investigate the coordinated operation of HES during such conditions.

VI. REFERENCES

[1]X. Jin et al., "Exploring the transition role of cascade hydropower in 100% decarbonized energy systems," Energy, vol. 279, p. 128086, Sep. 2023, doi: 10.1016/j.energy.2023.128086.

[2] Q. Qian and P. Lin, "Safety risk management of underground engineering in China: Progress, challenges and strategies," J. Rock Mech. Geotech. Eng., vol. 8, no. 4, pp. 423–442, Aug. 2016, doi: 10.1016/j.jrmge.2016.04.001.

[3] J. Zhang, C. Cheng, S. Yu, H. Wu, and M. Gao, "Sharing hydropower flexibility in interconnected power systems: A case study for the China Southern power grid," Appl. Energy, vol. 288, p. 116645, Apr. 2021, doi: 10.1016/j.apenergy.2021.116645.

[4] O. Bamisile et al., "Environmental impact of hydrogen production from Southwest China's hydro power water abandonment control," Int. J. Hydrog. Energy, vol. 45, no. 46, pp. 25587–25598, Sep. 2020, doi: 10.1016/j.ijhydene.2020.06.289.

[5] K. Ma, J. Zhang, Z. Zhou, and N. Xu, "Comprehensive analysis of the surrounding rock mass stability in the underground caverns of Jinping I hydropower station in Southwest China," Tunn. Undergr. Space Technol., vol. 104, p. 103525, Oct. 2020, doi: 10.1016/j.tust.2020.103525.

[6] Y. Hu, W. Huang, J. Wang, S. Chen, and J. Zhang, "Current status, challenges, and perspectives of Sichuan's renewable energy development in Southwest China," Renew. Sustain. Energy Rev., vol. 57, pp. 1373–1385, May 2016, doi: 10.1016/j.rser.2015.12.138.

[7] L. Jiang et al., "Growth in Wind and Sun: Integrating Variable Generation in China," IEEE Power Energy Mag., vol. 13, no. 6, pp. 40–49, Nov. 2015, doi: 10.1109/MPE.2015.2458754.

[8] Y. Qiu, J. Lin, F. Liu, Y. Song, G. Chen, and L. Ding, "Stochastic Online Generation Control of Cascaded Run-of-the-River Hydropower for Mitigating Solar Power Volatility," IEEE Trans. Power Syst., vol. 35, no. 6, pp. 4709–4722, Nov. 2020, doi: 10.1109/TPWRS.2020.2991229.

[9] X. Cheng, Y.-L. Tang, J. Liu, H. Zhong, W.-W. Li, and Y.-L. Wu, "Ultrashort-Term Scheduling of Interbasin Cascaded Hydropower Plants to Rapidly Balance the Load Demand," IEEE Access, vol. 8, pp. 32737–32756, 2020, doi: 10.1109/ACCESS.2020.2973680.

[10] J. Li et al., "Operation Rules Optimization of Cascade Reservoirs Based on Multi-Objective Tangent Algorithm," IEEE Access, vol. 7, pp. 161949–161962, 2019, doi: 10.1109/ACCESS.2019.2948939.

[11] Y. Yu, Y. Wu, and Q. Sheng, "Optimal Scheduling Strategy of Cascade Hydropower Plants Under the Joint Market of Day-Ahead Energy and Frequency Regulation," IEEE Access, vol. 9, pp. 87749–87762, 2021, doi: 10.1109/ACCESS.2021.3071491.

[12] C. Su, W. Yuan, C. Cheng, P. Wang, L. Sun, and T. Zhang, "Short-term generation scheduling of cascade hydropower plants with strong hydraulic coupling and head-dependent prohibited operating zones," J. Hydrol., vol. 591, p. 125556, Dec. 2020, doi: 10.1016/j.jhydrol.2020.125556.

[13] Y. Feng, J. Xu, Y. Hong, Y. Wang, Z. Yuan, and C. Wang, "Reservoir Scheduling Using a Multi-Objective Cuckoo Search Algorithm under Climate Change in Jinsha River, China," Water, vol. 13, p. 1803, Jun. 2021, doi: 10.3390/w13131803.

[14] Y. Ma et al., "Decentralized monthly generation scheduling of cascade hydropower plants in multiple time scale markets," Int. J. Electr. Power Energy Syst., vol. 135, p. 107420, Feb. 2022, doi: 10.1016/j.ijepes.2021.107420.

[15] S. Yu, J. Shen, J. Zhang, and C. Cheng, "Optimal bidding for large-scale hydropower stations serving multiple power grids in multi-regional monthly electricity markets," Int. J. Electr. Power Energy Syst., vol. 147, p. 108836, May 2023, doi: 10.1016/j.ijepes.2022.108836.

[16] Y. Zhou, J. Zhao, and Q. Zhai, "100% renewable energy: A multi-stage robust scheduling approach for cascade hydropower system with wind and photovoltaic power," Appl. Energy, vol. 301, p. 117441, Nov. 2021, doi: 10.1016/j.apenergy.2021.117441.

[17] J. Xie, Y. Zheng, X. Pan, Y. Zheng, L. Zhang, and Y. Zhan, "A Short-Term Optimal Scheduling Model for Wind-Solar-Hydro Hybrid Generation System With Cascade Hydropower Considering Regulation Reserve and Spinning Reserve Requirements," IEEE Access, vol. 9, pp. 10765–10777, 2021, doi: 10.1109/ACCESS.2021.3049280.

[18] H. Wei, Z. Hongxuan, D. Yu, W. Yiting, D. Ling, and X. Ming, "Short-term optimal operation of hydro-wind-solar hybrid system with improved generative adversarial networks," Appl. Energy, vol. 250, pp. 389–403, Sep. 2019, doi: 10.1016/j.apenergy.2019.04.090.

[19] S. Zhou et al., "A novel multi-objective scheduling model for grid-connected hydro-wind-PV-battery complementary system under extreme weather: A case study of Sichuan, China," Renew. Energy, vol. 212, pp. 818–833, Aug. 2023, doi: 10.1016/j.renene.2023.05.092.

[20] X. Jin, B. Liu, S. Liao, C. Cheng, and Z. Yan, "A Wasserstein metric-based distributionally robust optimization approach for reliable-economic equilibrium operation of hydro-wind-solar energy systems," Renew. Energy, vol. 196, pp. 204–219, Aug. 2022, doi: 10.1016/j.renene.2022.06.118.

[21] M. Zhao et al., "Flexibility evaluation of wind-PV-hydro multi-energy complementary base considering the compensation ability of cascade hydropower stations," Appl. Energy, vol. 315, p. 119024, Jun. 2022, doi: 10.1016/j.apenergy.2022.119024.

[22] W. Luo, H. Jiang, S. Dai, Y. Chen, Z. Sun, and Z. Zhang, "Study on Cascade Hydropower Stations Coordinated Optimal Scheduling Model Considering Transmission Section Capacity Limitation and Target Generation," in 2018 2nd IEEE Conference on Energy Internet and Energy System Integration (EI2), Oct. 2018, pp. 1–6. doi: 10.1109/EI2.2018.8582506.

[23] Z. Feng, W. Niu, X. Cheng, J. Wang, S. Wang, and Z. Song, "An effective three-stage hybrid optimization method for source-network-load power generation of cascade hydropower reservoirs serving multiple interconnected power grids," J. Clean. Prod., vol. 246, p. 119035, Feb. 2020, doi: 10.1016/j.jclepro.2019.119035.

[24] Z. Feng, W. Niu, and C. Cheng, "Optimal allocation of hydropower and hybrid electricity injected from inter-regional transmission lines among multiple receiving-end power grids in China," Energy, vol. 162, pp. 444–452, Nov. 2018, doi: 10.1016/j.energy.2018.08.045.

[25] B. Liu, T. Liu, S. Liao, H. Wang, and X. Jin, "Short-term operation of cascade hydropower system sharing flexibility via high voltage direct current lines for multiple grids peak shaving," Renew. Energy, vol. 213, pp. 11–29, Sep. 2023, doi: 10.1016/j.renene.2023.05.095.

[26] W. Yuan, W. Xin, C. Su, C. Cheng, D. Yan, and Z. Wu, "Cross-regional integrated transmission of wind power and pumped-storage hydropower considering the peak shaving demands of multiple power grids," Renew. Energy, vol. 190, pp. 1112–1126, May 2022, doi: 10.1016/j.renene.2021.10.046.

[27] P. Wang et al., "Short-term optimal scheduling of cascade hydropower plants shaving peak load for multiple power grids," Renew. Energy, vol. 184, pp. 68–79, Jan. 2022, doi: 10.1016/j.renene.2021.10.079.

[28] X. Ma et al., "Optimizing pumped storage hydropower for multiple grid services," J. Energy Storage, vol. 51, p. 104440, Jul. 2022, doi: 10.1016/j.est.2022.104440.

[29] S. Liao et al., "Daily peak-shaving model of cascade hydropower serving multi-grids considering an HVDC channel shared constraint," Renew. Energy, vol. 199, pp. 112–122, Nov. 2022, doi: 10.1016/j.renene.2022.08.156.

[30] X. Ge et al., "Daily peak shaving operation of mixed pumped-storage hydro plants considering cascade hydraulic coupling," Energy Rep., vol. 9, pp. 971–978, Oct. 2023, doi: 10.1016/j.egyr.2023.05.207.

[31] L. Pan, X. Xu, J. Liu, and W. Hu, "Adaptive robust scheduling of a hydro/photovoltaic/pumped-storage hybrid system in day-ahead electricity and hydrogen markets," Sustain. Cities Soc., vol. 95, p. 104571, Aug. 2023, doi: 10.1016/j.scs.2023.104571.

[32] Y. Zhao, X. Chen, Q.-S. Jia, X. Guan, S. Zhang, and Y. Jiang, "Long-Term Scheduling for Cascaded Hydro Energy Systems With Annual Water Consumption and Release Constraints," IEEE Trans. Autom. Sci. Eng., vol. 7, no. 4, pp. 969–976, Oct. 2010, doi: 10.1109/TASE.2010.2050139.

[33] Z. Luo, W. Gu, Z. Wu, Z. Wang, and Y. Tang, "A robust optimization method for energy management of CCHP microgrid," J. Mod. Power Syst. Clean Energy, vol. 6, no. 1, pp. 132–144, Jan. 2018, doi: 10.1007/s40565-017-0290-3.

[34] H. Zhang, D. Yue, and X. Xie, "Robust Optimization for Dynamic Economic Dispatch Under Wind Power Uncertainty With Different Levels of Uncertainty Budget," IEEE Access, vol. 4, pp. 7633–7644, 2016, doi: 10.1109/ACCESS.2016.2621338.

[35] Z. Li, R. Ding, and C. A. Floudas, "A Comparative Theoretical and Computational Study on Robust Counterpart Optimization: I. Robust Linear Optimization and Robust Mixed Integer Linear Optimization," Ind. Eng. Chem. Res., vol. 50, no. 18, pp. 10567–10603, Sep. 2011, doi: 10.1021/ie200150p.

[36] H. Xing and X. Sun, "Distributed Generation Locating and Sizing in Active Distribution Network Considering Network Reconfiguration," IEEE Access, vol. 5, pp. 14768–14774, 2017, doi: 10.1109/ACCESS.2017.2732353.

[37] Y. Zhou, H. Yu, Z. Li, J. Su, and C. Liu, "Robust Optimization of a Distribution Network Location-Routing Problem Under Carbon Trading Policies," IEEE Access, vol. 8, pp. 46288–46306, 2020, doi: 10.1109/ACCESS.2020.2979259.

[38] L. Lu et al., "Optimization model for the short-term joint operation of a grid-connected wind-photovoltaic-hydro hybrid energy system with cascade hydropower plants," Energy Convers. Manag., vol. 236, p. 114055, May 2021, doi: 10.1016/j.enconman.2021.114055.

HONG ZHOU is with Southwest Branch of State Grid Corporation of China. His research interests include large-scale power grid planning and operation, optimal scheduling of cascade hydropower station, and renewable energy resources.

LIANG LU was born in 1984. He is a senior engineer in the Southwest Branch of State Grid Corporation of China. His research interests include large-scale power grid planning and operation, optimal scheduling of cascade hydropower station, and renewable energy resources.

MINGKUI WEI was born in 1970. He is a senior engineer in the Southwest Branch of State Grid Corporation of China. His research interests include large-scale power grid planning and operation and peak load management.

LI SHEN is with Southwest Branch of State Grid Corporation of China. His research interests include large-scale power grid planning and operation and peak load management.

YOUBO LIU (M'15) received the Ph.D. degree in College of Electrical Engineering from Sichuan University, China in 2011. He is a Professor in the College of Electrical Engineering, Sichuan University, China. His research interests include operation control of power distribution system, smart grid and power market.